Star-shaped conformers generated by co-evolutionary docking predict cross-fitting glycoprotein trimer pre-fusion interfaces on VHSV fish rhabdovirus

short title: co-evolutionary docking to VHSV fusion

Coll, J*.
*Department of Biotechnology. Centro Nacional INIA-CSIC. Madrid, Spain.
*Julio Coll, orcid: 0000-0001-8496-3493
Email: juliocollm@gmail.com & julio.coll.m@inia.csic.es (JC)
* Corresponding author

Abstract

Despite the abundant diseases caused by rhabdoviruses on plants, animals and men, there are no approved therapeutic drugs. This work targeted viral hemorrhagic septicemia viruses (VHSV), a group of representative rhabdoviruses causing devastating world-wide diseases on fish farmed-species. In particular, their glycoprotein (gpG_{VHSV}) trimers were computationally targeted at its earliest pre-fusion inner interface. Co-evolution initiated from an optimized 2D-molecular parent and the corresponding gpG_{VHSV} -conformer 3D cavity, generated tens of thousands of raw-children, and selected hundreds of cross-fitting conformer variations in a few scaffolds. Their predicted drug-like high affinities in nanoMolar ranges, low toxicities and targeting the pre-fusion inner interface were confirmed by independent algorithms.

Keywords: Co-evolutionary docking; rhabdovirus: vesicular stomatitis, rabies, fish rhabdoviruses, VHSV, IHNV, SVCV, VSV, CHAV

Introduction

Rhabdoviruses are spreaded worldwide among vertebrates (mammals, birds, reptiles, fish), invertebrates (insects, arachnids, crustaceans) and plants. Some rhabdoviruses cause pathologies in humans (i.e., rabies, CHAV), and farmed (i.e., VSV, VHSV, IHNV, SVCV) wild-animals (i.e., rabies, VHSV). However, despite being known during decades, there are not yet any therapeutic drugs approved for rhabdoviral infections.

Because of previous work, the **v**iral **h**emorrhagic **s**epticemia **v**irus (VHSV) has been chosen here as one of the fish rhabdoviruses example to computationally explore for possible drug-like alternatives. Isolated from > 65 fish species (~ 20 farmed)[1], and increasingly found in free-living marine fish species [2], VHSV causes one of the highest economic impacts in fish farming. Many VHSV isolated world-wide have been grouped into 4 nucleoprotein genotypes with 9 subtypes (https://aphis.prod.usda.gov/livestock-poultry-disease/aquaculture/viral-hemorrhagic-septicemia).

Morphologically, VHSVs are typically bullet-shaped, membrane-enveloped virions like other rhabdoviruses. As most rhabdoviral genomes, VHSVs are encoded by ~11 Kb single-stranded, unsegmented and negative polarity RNA genomes (complementary to mRNA). The VHSV genomes codes for 5 structural and 1 non-virion proteins like any other *Novirhabdoviruses*[3, 4]. The genome is surrounded by viral proteins and enveloped by a membrane spiked with glycoprotein (gpG_{VHSV}) trimers. Their membrane virion surface contains ~ 300 trimeric spikes of ~ 500 amino acid glycoprotein G (gpG_{VHSV}), that recognizes host-dependent cellular receptors. After being internalized, the host intracellular endosomal low-pH mediates fusion of viral / endosomal membranes facilitating the release of the VHSV genome into the host cytoplasm whose biomachinery starts viral RNA translation and transcription to replicate new virions.

Like in any other rhabdoviruses, the gpG_{VHSV} is the only viral protein targeted by neutralizing host antibodies and the most used vaccine targeted[5]. In salmonids, intramuscularly injected DNA-vaccines coding for gpG_{VHSV} as well as for other gpG fish *Novirhabdoviruses,* have shown 80-100 % protection against homologous rhabdoviral challenges. The success of these prevention methods allowed the approval of the APEX-IHN DNA-vaccine for salmonid farming at North America [6]. However, similar DNA-vaccines against other fish rhabdoviruses have not been equally protective (i.e., SVCV in carp). There are no high-affinity therapeutic drugs approved to stop rhabdoviral outbreaks in salmonid farms.

Although the gpG_{VHSV} conserve similar folded domains, disulphide-bonding pattern and trimers among rhabdoviruses[7], their amino acid sequences are not conserved (< 20 % of identity). Therefore, there no cross-neutralization, nor antigenic relationships among rhabdoviruses[8], reducing the expectations for any universal rhabdoviral vaccine and/or possible unique therapeutic drugs.

The crystal homotrimeric structures of the ectodomain (residues 1–422) of the mammalian rhabdovirus **v**esicular **s**tomatitis **v**irus (VSV) gpG_{VSV}, were already reported on 2006-2007[9, 10]. Both pre- (physiological pH) and low-pH induced post-fusion conformations were crystallographic solved for gpG_{VSV} isolated by proteolisis of purified VSV virions. According to more recent crystallographic evidences derived from the **Cha**ndipura **v**irus (CHAV)[11, 12] and **rab**ies **v**irus (RABV)[13], each mammalian gpG chain folds into fusion (**FD**), pleckstrin-homology (**PH**), and trimerization (**TrD**) domains. Shorter **R1-R5** linkers connect the domains (**Figure S1** and **Table S2**)[3, 4, 25-28]. At the virion membrane surface, the gpG_{VSV} monomeric chains folded into pre-fusion homotrimers[17] around a central top-to-bottom cavity (**Figure S1**). At the virion membrane surface, the lowering of pH triggers extensive conformational gpG_{VSV} changes by refolding several **R**-linkers. By spring-loaded mechanisms, short α-helices of some **R**-linkers extend and refold favoring relative rotations between domains and induction of rigid six-α-helix bundles in the final post-fusion conformation, while maintaining the central trimer cavity. These mammalian rhabdoviral pre-to-post-fusion changes occur through reversible trimer-monomer-dimer-trimer pathway transitions[11, 12], in contrast to the irreversibility of other enveloped viral gpGs. Particularly in gpG_{VSV}, the low-pH induces refoldings of the **R1, R5** and **R4** linkers contributing to relative position changes of **FD** / **TrD** and extending the **TrD** α-helices from a **R4-TrD** interface (**Figure S1, Figure 1**). The protonation of ^{60}H, ^{162}H, ^{407}H and ^{409}H gpG_{VSV} residues may constitute sensitive pH switches to favour separation of **R5** / **FD** towards their post-fusion conformation[14]. At physiological high-pH, deprotonation of ^{268}D, ^{274}D, ^{395}D, and ^{393}D (and/or other acidic residues at **R4 / R5**), could destabilize the post-fusion six-α-helix-bundles, favouring a back transition to their previous pre-fusion conformations[15]. Many of those folding / fusion features were confirmed by the corresponding mutagenesis studies. Despite their amino acid sequence discrepancies, the trimer, 3-domain monomer folding (including disulphide pattern and Cystein domain borders), linkers and pH-dependent refolding transitions, were very similar among mammalian rhabdoviruses, whether gpG were obtained by virion protease digested gpG_{VSV} or gpG_{CHAV} [9, 10, 11, 12] or recombinant gpG_{RABV}[13]. However, such features are not yet completely understood for other rhabdoviruses.

Limited evidence of similar folding / fusion features such as those commented above, are available for gpG_{VHSV}. Nevertheless, the mapping of discontinuous epitopes on gpG_{VHSV} of VHSV-specific neutralizing monoclonal antibodies [16, 17], and the results of some mutagenesis studies affecting gpG_{VHSV} -dependent fusion[18] confirmed some similarities. Additionally, gpG_{VHSV} / gpG_{VSV} pepscan peptides displayed homologous locations for anionic phospholipid-bindings[19], for induction of interferon [20] or activation of autophagy [21]. Therefore, the present working hypothesis was that the gpG_{VHSV} main folds and earliest fusion transitions, were similar to those of the gpGs of mammalian rhabdoviruses. In particular, the main purpose of this computational work was to explore the sequence-conserved **R4-TrD** interface at the pre-fusion gpG_{VHSV} homotrimers (**Supporting Materials / 89VHSValignement.docx**).

Neither any gpG domain, nor peptides, nor small drug-like molecules, have been reported to inhibit the low-pH induced transitions in rhabdoviruses, in contrast to other enveloped viruses (i.e., human respiratory syncytial virus)[22]. Nevertheless, some antiviral compounds of broad-spectrum inhibiting salmonid IHNV rhabdovirus by targeting their phospholipids have been proposed [23]. More recently, natural extracts with limited affinities against SVCV infections have been proposed, such as, arctigenin (*F. Arctii*), bavachin (*P. corlifonia*), saikosaponin (*B. yinchowense*) and anisomycin (*S. griseolus)* or semi-synthetic derivatives from arctigenin[24], coumarin[25] and quinoline[26]. Therefore, high-affinity, low-toxicity (low environmental risks) drug-like small molecules to interfere VHSV rhabdoviral outbreaks or further investigate their fusion mechanisms, would be most welcome.

To computationally explore drug-like anti-gpG_{VHSV}, large numbers of high-affinity 3D-conformers docking to gpG_{VHSV} need to be generated. For that, the fastest java-based ***D**ata**W**arrior **B**uild **E**volutionary **L**ibrary* (DWBEL)[2-5] algorithms were employed. To start DWBEL co-evolutions, 2 optimal inputs were required: **i)** a 2D-molecular parent (to randomly generate large numbers of raw-children) and **ii)** a docked gpG_{VHSV}-parent complex target cavity (to evaluate DWBEL-3D-conformers). Once optimized the 2 inputs, co-evoluted generations originated tens of thousands of raw-children. Each raw-children was then evaluated for fitness to the target cavity (and other user-defined criteria), to select best-fitted children DWBEL-conformers. Iterations yielded hundreds of unique DWBEL-conformers with increased affinities [6, 7, 8-11], for independent **A**uto**D**ock**V**ina (ADV) docking[27, 28], to generate additional ADV-conformers to confirm increased affinities and targeted cavities.

Computational Methods

Modeling of gpG$_{VHSV}$

The gpG$_{VHSV}$ from 89 amino acid sequences of different VHSV isolates from diverse world-wide sources were aligned by Clone Manager vs9. The ^{67}EFEDIN and ^{302}LNHLIT amino acid sequences around the **R4**-linker and the **TrD** showed only one (I71T) or three (N203G) mutations, respectively (**Supporting Materials / 89VHSValignement.docx**).The gpG$_{VHSV}$ amino acid sequences were aligned to gpG$_{VSV}$ and other rhabdoviruses, maximizing Cystein and the most important amino acid sequences implicated in the gpG$_{VSV}$ fusion transitions (**Table S2**)[29, 9, 10]. The crystallographic gpG$_{VSV}$ ectodomain RCBS-PDB models (5I2S for pre-fusion and 5I2M for post-fusion), were employed as templates to Swiss model the gpG$_{VHSV}$ sequence (VHSV07.71 of 507 amino acids from UniProtKB P27662, GLYCO_VHSV0) (https://swissmodel.expasy.org/interactive). Previously to the modeling, the corresponding homotrimer structures were generated from the original pdb files containing crystallographic information (PyMol/A/Generate/ symmetry mates/within 4 Å). The Swiss-modeling was preferred to alphafold because of similar monomer[30] and best pre-fusion homotrimer structure predictions.

Generation of gpG$_{VHSV}$ DWBEL-conformers

Thousands of unique children were randomly generated by the co-evolution algorithms provided by **D**ata**W**arrior-**B**uild **E**volutionary **L**ibrary (DWBEL). DWBEL-conformers were selected to computationally target the gpG$_{VHSV}$ **R4-TrD** interface. To initiate DWBEL, the selection of an appropriated 2D molecule as initial parent proved to be not trivial. After preliminary dockings to manually designed hypothetical ligands, the highest affinities to the **R4-TrD** interface inner cavity were predicted by those molecules with 3-fold star-shaped conformers simultaneously docking to gpG$_{VHSV}$ amino acids located at their 3 chains rather than only at 1 or 2 chains. Alternative 3-fold star-shaped 2D molecules were manually designed with different central atoms / rings and arm sizes between 1-6 carbons. The **c**onformer **n**umber 30 (cn30) (**Figure 3B**), was chosen as parent (**Supporting Materials / StarShapedLigands.dwar**) and the gpG$_{VHSV}$-cn30 **R4-TrD** as target cavity for DWBEL.

Additional co-evolution preference criteria were, fitting the cavity using a relative maximal weight of 4, MW <= 600 g/mol (weight 2) and hydrophobicity LogP <=4 (weight 1) (to limit children unspecificities) and Toxicity risk <=1 (weight 4) (to minimize toxicity risks during co-evolution). To perform DWBEL the optimal mmff94s**+** force-field algorithm[31] was chosen. The DWBEL co-evolution generations randomly added/inserted small molecular variations into the 2D cn30 to originate tens of thousands of raw-children that were consecutively numbered (ID) (**Figure S2**). Each raw-children was evaluated for fitness not only to the provided target cavity, but also to the user-defined criteria. The DWBEL evaluation discarded the non-fitting and selected the best-fitted children DWBEL-conformers. The processes were repeated during several runs of hundreds of generations per run, to yield hundreds of unique non-toxic best-fitted children DWBEL-conformers with increased cavity-specificities[6, 7, 8-11]. To prepare for ADV docking, the non-toxic fitted-children were further filtered to exclude any mutagenesis, tumorigenicity, reproductive interference, irritant molecular signatures, and/or nasty functions that had survived the co-evolution, by screening hundreds of those toxic possibilities36. The final output of hundreds of non-toxic fitted-children DWBEL-conformers ordered by their generation were renumbered by their affinities (NN) and saved as *.sdf 3D files including their mmff94s**+** minimization conformers[37] to preserve their 2D geometries. This minimization step proved to be essential for optimal PyMol visualization (using the split_states PyMol command)[32] and to increase the accuracy and reproducibility of ADV docking[32].

Confirmation by gpG$_{VHSV}$ ADV-conformers

The **A**uto**D**ock**V**ina (ADV) [46] algorithms (available at the PyRx-0.98/1.0 package) were employed to **i)** compare affinities between ADV and DWBEL-conformers, **ii)** quantify ADV-conformer affinities in ~ nM, **iii**) identify PyMol nearby amino acids in docked complexes between gpG$_{VHSV}$ and ADV-conformers[32-35] and **iv)** confirm the gpG$_{VHSV}$ cavities targeted by ADV-conformers. The ADV algorithm was selected among the numerous alternative docking programs because of higher accuracies and ongoing improvements [27, 28, 36, 37]. The PyRx/Obabel/ADV algorithms were adapted to large scale docking requirements[38, 39]. Previous to ADV docking, non-toxic fitted-children DWBEL-conformers were minimized using the mmff94s**+** force-field to conserve their 2D-structures. Additional minimizations were performed by PyRx/OpenBabel mmff94s before the conversion to *.pdbqt files[40] required for ADV docking. The input children DWBEL-conformers (ID by their generation number) were renumerated (NN by their affinities) before ADV docking.

A 15x15x15 Å (15x) grid centered at the **R4-TrD** interface was employed to optimize the target cavity of the parent candidates described above. A wider grid of 45x45x45 Å (45x) centered to the PyMol / centerofmass, surrounding most of the pre-fusion gpG$_{VHSV}$ homotrimer (~ blind-docking) was employed to confirm affinity and **R4-TrD** target of the ADV-conformers. Because of the large numbers of children, only the best-fitting ADV-conformer of 9 possible per child was selected for further studies. The corresponding output ADV-conformer docking-scores in - Kcal/mol[41, 34, 42, 43] were converted to ~ nM affinities by the formula, 10^{9}-(exp$^{(Kcal/mol/0.592)}$).

To identify the gpG$_{VHSV}$ amino acids nearby 4 Å distance of each ADV-conformer, a Python script was designed to be run in PyMol-opened gpG$_{VHSV}$.pdb files . Preliminary ADV docking results were employed to define each of the gpG$_{VHSV}$ cavities by their most frequently docked 3 amino acids. The defined gpG$_{VHSV}$ cavities were: **Bc** (at the bottom of the **TrD** α-helix)**:** 317D and/or 320S and/or 335K, **R4-TrD** (at the **R4-TrD** interface): 67E and/or 304H and/or 307T and **Sc** (at the trimer side-cavities): 296T and/or 366S and/or 411Y. The percentages of cavities targeted by thousands of ADV-conformers were approximated using a PyMol/Python script. Such script calculated the cavity percentages by the formula, 100 * number of ADV-conformers in each cavity / total numbers of docked ADV-conformers (**Supporting Materials / nearby11.py**). Due to some overlapping, the resulting approximations accounted for ~75-90 % of the total numbers of ADV-conformers.

Results

Some of the expected conformational changes induced by low-pH in the gpG$_{VHSV}$ pre-fusion homotrimer include the following similarities to gpG$_{VSV}$: **i) TrD** α-helix (**Figure 1, red**) extension by refolded **R4-**linkers (**Figure 1 green**), **ii**) **R5-** linker α-helix extension/reorientations (**Figure 1, yellow**), and **iii) R1-**linker refoldings to lateral α-helices (**Figure 1, blue**). Among all the above mentioned theoretical possibilities to interfere, the highly conserved pre-fusion homotrimer **R4-TrD** interface of gpG$_{VHSV}$ was chosen as the working hypothesis to computationally interfere the fusion transitions at one of its earliest steps.

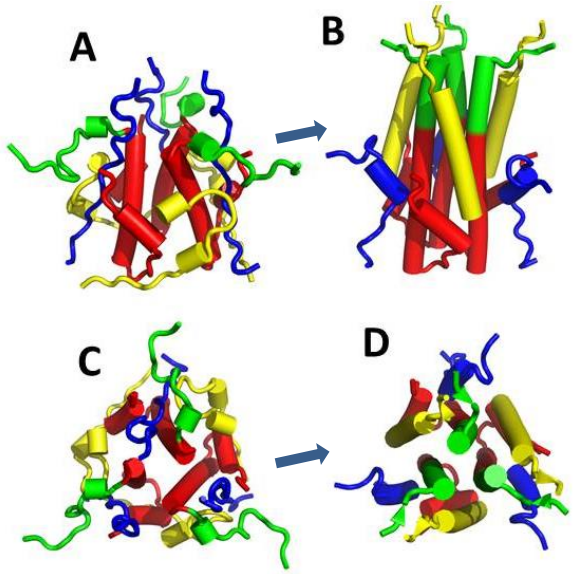

Figure 1
Low-pH-induced gpG$_{VSV}$ transitions (→) from pre-(AC) to post-(BD) fusion conformations
The gpG$_{VSV}$ homotrimer ectodomain sequences implicated in fusion were extracted from 5I2S and 5I2M models in PyMol, their α-helices were drawn as cylinders (gpG$_{VSV}$ whole ectodomains at **Figure S1**). The corresponding folds, Cysteins and trimers in gpG$_{VHSV}$ were similar but differed in their amino acid sequences (**Table S1**). **A**,**B**,) gpG$_{VSV}$ side views. **C**,**D**) gpG$_{VSV}$ top views
A,**C**), extracted from the gpG$_{VSV}$ 5I2S.pdb pre-fusion modeled at physiological high-pH [10]
B,**D**), extracted from the gpG$_{VSV}$ 5I2M.pdb post-fusion modeled at endosomal low-pH [9].
Blue cartoons, **R1**-linkers. **Green cartoons**, **R4**-linkers. **Red cartoons**, invariable central **TrD** α-helix gpG$_{VSV}$ residues 273-309. **Yellow cartoons**, **R5**-linkers

Searching for appropriated 2D-molecules to start DWBEL, numerous preliminary ADV docking attempts resulted in limited conformer affinities to **R4-TrD** predicting docking to 1 or 2 chains of gpG$_{VHSV}$. Only a few manually designed star-shaped conformer candidates cross-docked the inner cavity at the level of **R4-TrD**. Such candidates were also chosen because they not only cross-docked the 3 chains but also occupied a central position in the inner cavity of the gpG$_{VHSV}$ pre-fusion trimer. Among a few other possibilities, the cross-docked conformer **n**umber 30 (cn30, chemical formula: C24H45N3O6), was selected for further work. The cn30 corresponded to an star-shaped 2D-molecule of a central cyclohexane with 3 symmetrical arms of 4 carbons each, ended by amine / carboxylic groups (Alanines), of 471 g/mol of molecular weight and -3.3 LogP hydrophobicity (**Figure 3, up**). In particular, the corresponding conformer of cn30 cross-docked the A,B,C chains of gpG$_{VHSV}$ implicating most of their ^{67}E, ^{68}F,^{71}I, ^{72}N, ^{302}L ^{303}N, ^{304}H, ^{307}T (amino acids defining the gpG$_{VHSV}$ **R4-TrD**) with low affinities around ~ 4400 nM**.** Therefore, to explore whether such affinities could be increased, DWBEL co-evolutions were attempted. To star DWBEL co-evolutions, the cn30 was chosen as parent to generate large numbers of raw-children and the gpG$_{VHSV}$-cn30 ADV docked complex cavity was chosen as target to select the best-fitting children DWBEL-conformers. As DWBEL controls for specificity, one cn30 parent was also chosen by maintaining constant its central cyclohexane-4 carbon arms, thus restricting their co-evolution to its terminal Alanines (fixed or restricted cn30).

Such above mentioned co-evolutions generated tens of thousands of raw-children with random small molecular changes. After numbered by their generation ID, the conformers that best-fitted the gpG$_{VHSV}$-cn30 cavity, molecular weight, hydrophobicity and non-toxicity-risk criteria, were retained for each generation. Consecutive generations of non-toxic best-fitted DWBEL-conformers were repeated during 2-4 consecutive runs of ~ 100 generations per run. Each run re-started co-evolution from cn30 avoiding raw-children duplicates. The affinities predicted by non-toxic best-fitting **R4-TrD** DWBEL-conformers (**Figure S2**, **blue circles)** were finally compared to affinities predicted by ADV-conformers. The ADV blind-docking was employed to identify those conformers which not only predicted higher affinities (**Figure S2, red circles**) but also conserve their **R4-TrD** cross-targeting DWBEL-conformers**.**

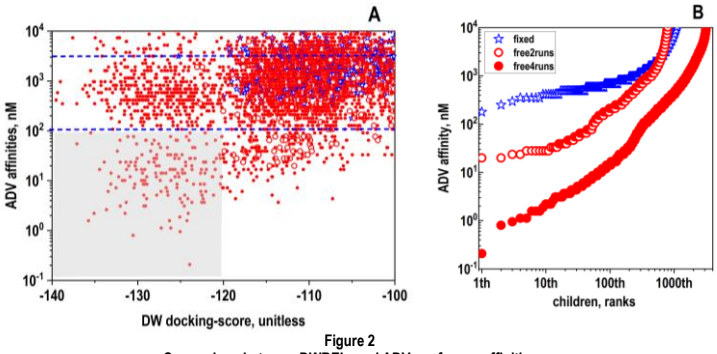

Figure 2
Comparison between DWBEL- and ADV-conformer affinities

DWBEL co-evolutions generated tens of thousands of raw-children. The number of selected non-toxic fitted-children DWBEL-conformers were 834 (2 runs) and 3313 (4 runs). For comparison, the cn30 parent (**Figure 3**) predicted -58.1 / 4400 nM conformer affinities, by DWBEL / ADV, respectively.
A, DWBEL- / ADV-conformer affinity comparison. **B,** rank profiles of ADV-conformers.
Horizontal blue-dashed lines, Affinities of ADV-conformer of cn30 (top line) and restricted-cn30 children (down line)
Gray rectangle, non-toxic top-children DWBEL- /ADV-conformers predicting < -120 / < 100 nM affinities, respectively
Blue stars, conformers derived by 3 runs from fixed or restricted-cn30.
Red open circles, conformers derived by 2 runs from free cn30.
Red solid circles, conformers derived by 4 runs from free cn30.

The cn30 and gpG$_{VHSV}$-cn30 co-evolution for 2-4 consecutive runs predicted some correlation trend between non-toxic fitted-children DWBEL-conformers and their corresponding ADV-conformers (**Figure 2A, red open** and **solid circles**). Additionally, most of the conformers predicted improvements in their DWBEL or ADV affinities compared to their initial cn30 parent. Also, the children generated by 4 runs predicted higher affinities (lower docking-scores) than those predicted by 2 runs (**Figure 2A, red solid** and **open circles,** respectively). In contrast, the affinities predicted by conformers generated from restricted-cn30 (**Figure 2, blue stars**) were closer to the cn30 affinity (**Figure 2A, horizontal top blue-dashed line** and **2B**). More details of the top-children of the 4 run coevolution are provided at **Supporting Materials / 549Children-gpGvhsv.dwar**.

To compare the cavity preferences of the ADV-conformers, the approximated percentage distribution of their targets were calculated among three pre-defined gpG$_{VHSV}$ cavities. Results showed that those top ADV-conformers predicting the highest docking affinities (~ 0.2-100 nM) (**Figure 2A, gray rectangle** and **2B, red solid circles**) targeted **R4-TrD** at the center of the trimer inner cavity cross-docking their 3 chains (33-37 %, n=834-3313 non-toxic fitted-children ADV-conformers, respectively) (**Figure 3A, red up arrow**). However, two additional docking cavities were also preferred by alternative ADV-conformers. Thus, some children that targeted **R4-TrD** by DWBEL-conformers, also targeted **Bc** by different ADV-conformers (**Figure 3A, red down arrow**). The wider grid of ADV compared to DWBEL, may explain such differences. About, 60-58 % of children ADV-conformers preferred **Bc** at the bottom of **TrD** α-helices, although with > 10-fold lower affinities than those children which cross-docked 3 chains at the **R4-TrD** interface (**Figure S3**). Additionally, an smaller percentage of ADV-conformers, preferred targeting to the sides (**Sc**) of the homotrimer (5-2 %) (**Figure 3A, red left arrow**).

Two ADV main-scaffolds were dominant among the top cross-docking ADV-conformers. The dominant scaffold was present in 70.3 % of the children while the rest of the children mostly predicted one secondary scaffold (as calculated by DW/Chemistry/ Analyse Scaffolds/Most central ring system). The top-child ID number 35399 (2860 NN), representative of the main scaffold, predicted star-like DWBEL- and ADV-conformers with one central bipartite cyclohexane/5-ring from which 3 arms ± rings expanded in symmetrical directions (**Figure 3B, top-child: 35399**). The 35399 docked most of the amino acids in the 3-chain side-cavities of the gpG$_{VHSV}$ **R4-TrD** interface (**Table 1**). The representative top-child of the secondary scaffold (4566 ID, 401 NN), predicted also an star-like conformation but with a unique central cyclohexane from which 3 arms ± rings expanded in symmetrical directions (**Figure 3B, top-child: 4566**).

Both 35399 and 4566 ID representative scaffolds predicted hundreds of molecular variants differentiated only by a few atoms, positions and/or rings. Detailed PyMol visualization of the gpG$_{VHSV}$ pre-fusion **R4-TrD** interface cross-docked to top-children DWBEL-conformers may be further explored at **Supporting Materials / 600Children-gpGvhsv.pse.** Top-children examples of the two representative scaffolds, predicted similar cross-dockings that might interfere with the interface between the amino terminal invariable α-helix of **TrD** (**Figure S4, red**) and the carboxy-terminal of the **R4** linker (**Figure S4, green**).

The predicted contacts to gpG$_{VHSV}$ amino acids of representative cross-docking top ADV-conformers were similar for both scaffolds. Most of their differences were from their hydrogen bond patterns. The ID 35399 and 4566 predicted their nearby amino acids at similar residues among the three **A**,**B** and **C** gpG$_{VHSV}$ homotrimer chains. Most of their main nearby amino acids were distributed among **R1** (^{67}E, ^{68}F, ^{71}I, ^{72}N), **R4** (^{302}L, ^{303}N. ^{304}H) and **TrD** (^{306}I, ^{307}T). The hydrogen bonds predicted for 35399 or 4566 were 4 (**B,C** chains) or 6 (**A,B,C** chains), respectively (**Table 1**).

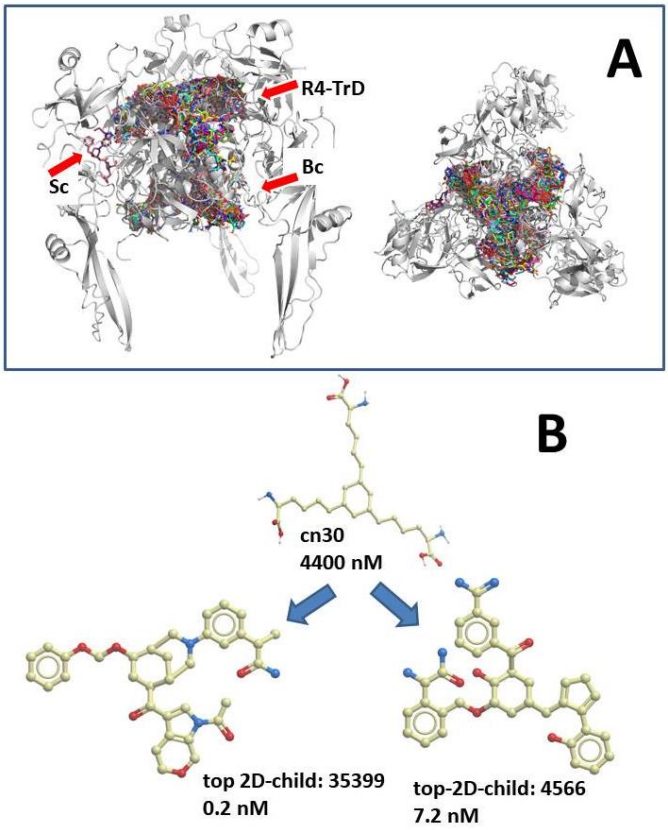

Figure 3
Top ADV-conformers cross-docking to gpG$_{VHSV}$ (A) and representative 2D top-scaffolds (B)

Four consecutive runs of DWBEL co-evolution generated 43065 unique raw-children. The resulting 3313 non-toxic fitted-children DWBEL-conformers were then ADV docked. The representative ADV 2D top-child scaffolds best-fitting the gpG$_{VHSV}$ **R4-TrD** interface were drawn in MolSoft (the IDs corresponded to the DWBEL generation and their ~nM affinities to the ADV-docking). DWBEL 35399 ID corresponded to ADV 2860 NN. DWBEL 4566 ID corresponded to ADV 401 NN. Top-children DWBEL- and ADV-600 conformers, molecular properties and affinities were supplied as a Table with selection sliders (**Supporting Materials / 600Children-gpGvhsv.dwar**).
A) Gray cartoons, gpG$_{VHSV}$ amino acid sequence side and top views.
Red arrows, ADV-conformer preferences distributed among **R4-TrD, Bc, Sc**
Multicolor sticks, 3313 ADV-conformers docked to gpG$_{VHSV}$ corresponding to 3313 DWBEL-conformers.
B) Red spheres, Oxygens. **Blue spheres**, Nitrogens. **Light green spheres and sticks**, Carbons and bonds..

Table 1
gpG$_{VHSV}$ amino acids nearby ADV cross-docked top-conformer representative scaffolds

Chain:residues gpG$_{VHSV}$			Aa	DWBEL ID (ADV NN): 35399 (2860)	4566 (401)
A:	67	E	GLU		
	68	F	PHE		H
	71	I	ILE		
	72	N	ASN		H H
	302	L	LEU		H
	303	N	ASN		
	304	H	HIS		
	306	I	ILE		
	307	T	THR		
B:	67	E	GLU		
	68	F	PHE		
	71	I	ILE		
	72	N	ASN		
	302	L	LEU		H
	303	N	ASN		
	304	H	HIS	H H	
	306	I	ILE		
	307	T	THR		
C:	67	E	GLU		
	68	F	PHE		H
	71	I	ILE		
	72	N	ASN		
	302	L	LEU	H	
	303	N	ASN		
	304	H	HIS	H	
	306	I	ILE		
	307	T	THR		

To automatize the identification of gpG$_{VHSV}$ amino acids to 4 Å distance of the top-children ADV-conformers, a Python script was designed to be run in PyMol. DWBEL 35399 ID corresponded to ADV 2860 NN. DWBEL 4566 ID corresponded to ADV 401 NN.
H, Hydrogen bonds identified by LigPlus.
Blue, R1. Green, R4. Red, TrD (Table S2).

https://doi.org/10.26434/chemrxiv-2024-xs262 **ORCID:** https://orcid.org/0000-0001-8496-3493

Discussion

This work describes non-toxic star-shaped conformers computationally targeting the conserved gpG_{VHSV} **R4**-linker / **TrD**-α-helix trimer pre-fusion interface predicting cross-docking at low nanoMolar affinities. The expectations were that some of them could interfere with some of the fusion conformational transitions to inhibit VHSV infection (~ mini-multivalent drugs?).

These computationally successful candidates were obtained by optimizing initial parent designs and complementary DWBEL and ADV docking algorithms. The first most important step was an intensive search for an specific initial 2D molecular parent from which to generate many derivatives whose ADV-conformers would computationally cross-fit the gpG_{VHSV} **R4-TrD** interface. After numerous testing alternative manual 2D designs, the highest docking affinities at low **µM** ranges were predicted only by 3-fold symmetry star-shaped ADV-conformers. Most of the higher affinity star-shaped conformers cross-docked the 3-chains which formed the **R4-TrD** inner-cavity of the gpG_{VHSV} pre-fusion trimer, rather than docking only to 1 or 2 chains. Aiming to improve their **µM** affinities and to maintain their cross-targeted **R4-TrD**, the cn30 was selected for further work. Tens of thousands of raw-children derivatives were randomly generated from the cn30 parent using DWBEL co-evolution. During their co-evolution, the gpG_{VHSV}-cn30 cavity was employed to screen for those best conformers fitting all the drug-like chosen criteria. Thousands of non-toxic children conformers with specific molecular weights, hydrophobicity and best-cross-fitting the **R4-TrD** interface were generated. The new children affinity improvements and maintenance of their cross-targets were confirmed by applying the ADV independent algorithm. Hundreds of unique top-children ADV-conformer candidates predicting affinities in the low nanoMolar range and cross-fitting the **R4-TrD** interface were identified. All those top-children predicted molecular conformers with many small variations of 3-arm star-shaped 2 main scaffolds, suggesting that high-affinity cross-docking of the 3 chains of trimeric gpG_{VHSV} **R4-TrD**, could be the best target to propose to interfere with fusion transitions. Although with similar limitations, these results were analogous to those predicted before for the SARS-CoV2 trimer employing also co-evolution strategies[44] .

Some of the limitations to the predicted molecules, include: **a)** hypothetical similarities between crystallographic-gpG_{VSV} and its modeled-gpG_{VHSV}, **b)** one parent 2D molecule and one **R4-TrD** targeted cavity were studied among many other possibilities (i.e., **Bc** / **Sc**, monomers, dimers, transition intermediates, etc), **c**) exploration of resistant mutations remains hypothetical, **d)** no consideration of **R4-TrD** side-chain amino acid flexibilities has been studied, and **e)** lack of experimental evidences, such as binding to recombinant gpG_{VHSV}, and/or inhibition of fusion (syncitia) or infectivity by VHSV *in vitro* / *in vivo* assays. On the other hand, despite the application of several improvements to the DWBEL-ADV algorithms by previous work in other protein / ligand pairs (**Table S1**) [48, 58, 45, 46, 38], further targeting the gpG_{VHSV} with alternative and deeper explorations, could add more penetration into the enormous chemical space[36, 39] . Most probably such efforts would increase the probabilities to identify distinct drug-like molecules, 3D conformers and scaffolds docking gpG_{VHSV}.Therefore, up to now all that can be said is that these top cross-docking conformers predicted high-affinity contacts to some of the gpG_{VHSV} amino acids implicated in one of the most probable earliest-steps of trimer fusion transitions.

During the last years small molecular weight drug-like compounds have been rarely proposed to treat rhabdovirus outbreaks on farmed fish (except those for IHNV vaccine prevention or SVCV natural products. Most probably, the risk of introducing toxicities on the aqueous environment could explain some of these delays. To computationally prevent those potential toxicity problems, the generated conformers were selected during and after their co-evolution to eliminate hundreds of known toxicities. However, on due time to further reduce the probability of environmental risks, experimental evidences would be needed. In the meanwhile, basic research on VHSV infection / fusion could benefit from the experimentation with some of these or similarly generated conformers.

Because of the large divergence of amino acid sequences, it remains to be proven whether similar conformers could be generated for the **R4-TrD** interfaces on other rhabdoviruses, such as mammalian VSV, rabies or Chandipura or fish VHSV isolates, IHNV or SVCV. As indicated by some preliminary results, one of the key steps, would be to find sequence-specific appropriated parent 2D molecules to start successful co-evolutions.

For any possible anti-virus drug development, the prediction of possible resistant mutations that may emerge during drug-treatments and their hypothetical solutions, would be most important. Although some resistant mutations may have deleterious effects on viral replication, such as demonstrated on human respiratory syncytial virus[22] . Nevertheless, the hundreds of top DW-BEL- and ADV-conformer candidates cross-docking to gpG_{VHSV} **R4-TrD,** raise the probabilities to find some against possible emergent mutations. Similar co-evolution screening attempts were described before on other protein / ligand pairs. For instance, co-evolved children docking to the new mutations in SARS-CoV2 omicron variants[44] , anti-coagulant co-evolved children affecting rat mutants but not humans[45] or screening co-evolved children against Tecovirimat-emergent resistant human monkeypox variants[47] .

Many of the drug-cavities investigated here by both DWBEL and ADV, mapped to the 3-fold-symmetric central cavity of the pre-fusion **R4-TrD** interface of the gpG_{VHSV} model. However, it was remarkable to discover alternative gpG_{VHSV} cavities targeted by other ADV-conformers of the same children ID that targeted the **R4-TrD** by DWBEL-conformers. Two new cavities were targeted by the new ADV-conformers to the TrD α-helix bottom (**Bc**) or to the trimer side (**Sc**) (**Figure 3A**). One possible explanation for these behaviors would be that the ADV were performed using wider grids than those to DWBEL. In the case of ADV, the corresponding DWBEL-conformers remained undetected because only the best ADV-conformers out of 9 generated were studied due to the hundreds of conformers. Although with lower affinities, the targeted **Bc** / **Sc** cavities may also be biologically significant, hypothetically implicating conformer-dependent multiple docking sites at gpG_{VHSV} for the same children. If experimentally successful, conformers targeting **R4-TrD** could be combined with those targeting **Bc** to make more difficult any possible emergence of resistant mutations. It remains to be proven whether or not the highest affinity ADV-conformers would be the only ones interfering with gpG_{VHSV} fusion.

The hundreds of top-children predicted different conformers with variations in their molecular atoms and/or rings, but maintaining only two main scaffolds (representative top-children IDs 35399 and 4566). In this work, the top-children defined by ordering by their ADV affinities predicted the main 35399 scaffold, however, similarly to what was commented above for different conformers, the secondary 4566 scaffold could also experimentally show anti-fusion properties.

Supplementary information

Table S1

Software, computational improvements and hardware used here for computational manipulations

name	version	Main use and references	url
DataWarrior	Updated 5.5.0 Windows/Linus	Evolutionary docking[34] Commercial ChemSpace	https://openmolecules.org/ datawarrior/download.html)
Toxicity & nasty macro	2023	Eliminate residual toxic / nastic fitted-children after co-evolution[46]	
Toxicity Risks	2023 Updated DataWarrior	Minimize toxic / nasty raw- children during co-evolution increasing specificity[38]	https://openmolecules.org/ datawarrior/download.html)
Babel & AutoDockVina	Home-adapted PyRx 098/1.0	Mmff94s force-field minimization & 2D conservation	https://pyrx.sourceforge.io/
ADV consensus	2023 2024	First attempted for Anti-bacterial [32, 44] grid conformer comparisons	http://dx.doi.org/10.26434/chemrxiv-2023-ld9d3 This work
2D geometry conservation	2023	DW saving-SD files corrected by mmff94s+ force field minimization [57]	
MolSoft	3.9 Win64bit	Easiest manipulations of sdf files 2D drawing	https://www.molsoft.com/download.html
PyMol	2.5.7.	Visualization of molecules PyMol-Python scripts to detect nearby atoms	https://www.pymol.org/ this work
Discovery Studio	21.1.1.0.20298	Visualization of 2D molecules Structure/geometry fixing	https://discover.3ds.com/discovery-studio-visualizer-download
OriginPro	2022 2024	Calculations and Figures Macros to handle large numbers of data	https://www.originlab.com/ this work
Home-made pseudoligands	2023	Pseudoligand parents for DWBEL co-evolutions[48]	
LigPlot	2.2.8.	Amino acid bonds of docked conformers[32]	https://www.ebi.ac.uk/thornton--rv/software/LigPlus/applicence.html
AMD Ryzen i9 computer	4 DDR4 x 32[48] Gb memory	47 CPU Computational hardware	https://www.pcspecialist.es/

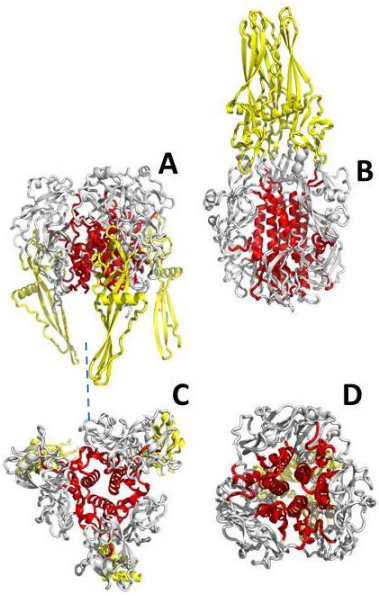

Figure S1
Crystallographic homotrimer models of gpG_{VSV} at their pre- and post-fusion conformations

Conformational transitions between the physiological or high-pH pre-fusion conformation (**A**,**C**) to their more compact endosomal low-pH post-fusion conformation (**B**,**D**). The transitions, extend existing α-helices with refolded ones forming a central bundle of 6 α-helices and rotating the fusion domain. The pH-dependent conformational transitions are reversible. In this work, the central internal cavity that runs both gpG_{VSV} conformations top to bottom has been computationally targeted using a gpG_{VSV}-modeled gpG_{VHSV} structure.

A, gpG_{VSV} **h**omotrimer pre-fusion side-view at high pH (5I2S). One of the hypothetical transmembrane has been drawn as a vertical dashed blue-line pointing towards the viral membrane.
B, gpG_{VSV} homotrimer post-fusion side-view at low pH (5I2M).
C, gpG_{VSV} pre-fusion top-view.
D, gpG_{VSV} pos-fusion side-view
Yellow cartoons, FD fusion domains
Red cartoons, TrD trimerization invariable α-helix domains and some **R** linkers implicated in the low-pH conformational changes that reorient the gpG_{VSV} conformational transitions

Table S2
Correspondence between gpG$_{VSV}$ and gpG$_{VHSV}$ amino acid domains and linkers

Name	explanation	Low-pH conformation	gpG$_{VSV}$	~ gpG$_{VHSV}$
R1	R1-linker	reversible α-helix	17-36	56-78
R2	R2-linker	Linker	46-53	88-95
FD	Fusion Domain	Re-oriented domain	54-172	96-212
R3	R3- linker	Linker	173-181	213-gap
PHD	~Pleckstrin Domain	Maintained fold	182-259	217-290
R4	R4-linker	Reversibly extended α-helix	**260-273**	**291-304**
TrD	Trimerization Domain	Whole trimerization domain	274-382	305-405
TrDhelix	α-helix of **TrD**	Invariable α-helix	**274-292**	**305-323**
R5	R5-linker	Reversibly extended α-helix	383-405	406-428

Amino acid gpG$_{VHSV}$ residues were aligned to gpG$_{VSV}$. Signal peptides, transmembrane and cytoplasmic tails were omitted. The invariable α-helix of **TrD** was separated from the rest of **TrD** to clarify targeting to the **R4-TrD** interface (bold numbers). Despite the low homology of their amino acid sequences, the gpG$_{VHSV}$ (in parenthesis) conserved most of the relative positions of the gpG$_{VSV}$ Cysteins such as ^{24}C (^{64}C), ^{68}C (^{110}C), ^{114}C (^{152}C), ^{153}C (^{192}C), ^{158}C (^{197}C), ^{177}C (^{215}C),^{219}C(^{251}C), ^{224}C (^{256}C), ^{253}C (^{285}C), and ^{284}C (^{315}C)[49] and their fusion hydrophobic bipartite tips ^{116}YA (^{154}WM) and ^{72}WY (^{114}FF). The 3D gpG$_{VHSV}$ model were Swiss-Modeled using 5i2s.pdb (physiological high-pH) and 5i2m.pdb (endosomal low-pH)[9, 10] gpG$_{VSV}$ as templates (RCSB Protein Data Bank, http://www.rcsb.org/pdb/home/home.do).

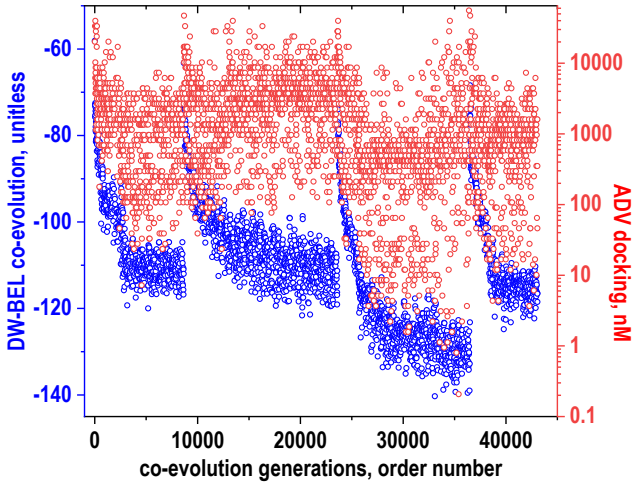

Figure S2
DWBEL-ADV affinities *vs* ID of non-toxic fitted-children during four consecutive runs

The DWBEL co-evolution randomly generated unique children restarting from cn30 in each of the 4 consecutive runs avoiding duplicates by keeping all results on the RAM memory (in our hands <100 Gb). The program assigned a consecutive ID order number for each raw-children generated. The fitted-children DWBEL-conformers are selected by fitting the gpG$_{VHSV}$ cavity and molecular weight, hydrophobicity and low toxic risk criteria. **Blue circles**, DWBEL unitless scores. **Red circles**, ADV best conformer ~ nM affinities.

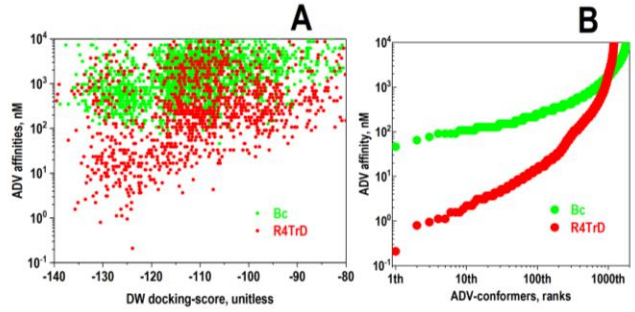

Figure S3
Comparison between DWBEL- and ADV-conformer affinities to Bc and R4-TrD cavities

The amino acid defined gpG$_{VHSV}$ cavities: **Bc** (at the **TrD** α-helix bottom) and **R4-TrD** (at the **R4-TrD** interface), identified the ADV-conformer targeted in gpG$_{VHSV}$ (**Supporting Materials / nearby11.py**). The ADV-conformer affinities and their corresponding DWBEL-conformer docking-scores were extracted from the 3313.sdf file data (**Figure 2, 4 runs**) using the Bc.txt and R4TrD.txt inputs from nearby11.py to the andrejlike3.py PyMol / Python script **(Supporting Materials / andrejlike3.py).**
A, affinities compared between DWBEL- and ADV-conformers targeting Bc/R4-TrD cavities.
B, rank profiles of the ADV-conformers targeting Bc and R4-TrD cavities.
Green circles, conformers targeting the **Bc** cavity.
Red circles, conformers targeting the **R4-TrD** interface cavity.

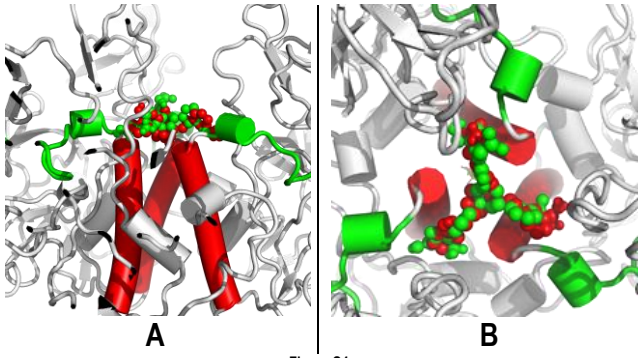

Figure S4
gpG$_{VHSV}$ prefusion R4-TrD interface docked to representative ADV top-children conformers
The representative top-ADV-conformers targeted the gpG$_{VHSV}$ interface between carboxy-terminal 304 residue of the **R4**-linker (**green**) and amino-terminal 305 residue of the invariable α-helix of the **TrD** (**red**). Similar targeting were shown by the corresponding top-DWBEL-conformers**.**
A, gpG$_{VHSV}$ side-view focused on the **R4-TrD** interface.
B, gpG$_{VHSV}$ top-view focused on the **R4-TrD** interface.
Red α-helix cylinders, pre-fusion **TrD** of 305-323 residues invariable α-helix.
Green cartoons, pre-fusion gpG$_{VHSV}$ **R4**-linker with its α-helix which will be refolded to α-helix at low-pH.
Gray cartoons, gpG$_{VHSV}$ amino acids around the **R4-TrD** interface.
Red spheres, top-child 3D conformer example of main 2D scaffold (~35399).
Green spheres, top-child 3D conformer example of secondary 2D scaffold (~4566).

Supporting Materials

- 89VHSValignement.docx. gpG$_{VHSV}$ from 89 amino acid sequences of different isolates from diverse sources were aligned by Clone Manager vs9. The ^{67}EFEDIN and ^{302}LNHLIT amino acid sequences around the **R4**-linker and the **TrD** were in **bold red** letters**.** Only one (I71T) or three (N203G) mutations (isolates in **red**), respectively were detected.

- StarShapedLigands.dwar Contains small star-shaped tripartite molecules manually designed by 2D drawing different central atoms / rings and sizes and 3-6 carbon arms ended by alanines. The designed 2D molecules were manually drawn in MolSoft. To conserve their 2D geometries during ADV docking, optimal conformers were generated by the DW / mmff94s**+** force-field algorithm[31] The best ADV conformer docking to gpG$_{VHSV}$ **R4-TrD** interface contacting all the A,B,C chains of the trimer, was conformer number 30 (cn30). The cn30 conformer was input parent and cavity for DWBEL co-evolution. Files *.dwar can be opened in DW, freely available at https://openmolecules.org/datawarrior/download.html

- 549Children-gpGvhsv.dwar. This *.dwar DW tables contain 549 top-3D conformers selected by their ADV affinities by 4-runs. The table is provided with threshold slider-filters to their DW_BEL and ADV docking-scores, Molecular weights and logP properties, to select for particular threshold combinations. Files *.dwar can be opened in DW, freely available at https://openmolecules.org/datawarrior/download.html

- nearby11.py. To compare the cavities preferentially targeted by thousands of new children-conformers, the percentages of docked cavities in gpG$_{VHSV}$ were approximated with the PyMol-Python script nearby11.py. The different gpG$_{VHSV}$ cavities were defined by their three most characteristic amino acids as: **Bc** (around the bottom-cavity at the end of the **TrD** helix) = 317D and/or 320S and/or 335K, **R4-TrD** (around the **R4-TrD** α-helix interface) = 67E and/or 304H and/or 307T and **Sc** (around the trimer side-cavities) = 296T and/or 366S and/or 411Y. The script calculated the percentages by the formula, 100 * number of children in each virtual cavity / total numbers of children docked. Copy all files into the same directory (*.py, gpG$_{VHSV}$ and output_number.pdbqt). Open the gpG$_{VHSV}$ file in PyMol and load the Python script by PyMol/File/Run Script/*.py.

- andrejlike3.py. PyMol-Python script to extract the ADV-conformer row data of a 3313.sdf file (including their DWBEL and ADV affinities) corresponding to **Bc** and **R4-TrD** txt files with the NN numbered conformers classified by their targeting to each of the cavities calculated by nearby11.py.

- 600Children-gpGvhsv.pse. Contains 600 top-children from DWBEL (runs=4) ADV docked to the gpG$_{VHSV}$ model ordered by from highest to lowest ADV affinities (~ 0.2-200 nM). To view the docked individual children click on the NN number to the right of the PyMol scene after opening the *.pse file in one of the latest PyMol 2023-24 versions.

Funding
The work was carried out without any external financial contribution

Competing interests
The author declares no competing interests

Authors' contributions
JC designed, performed and analyzed the computational work and drafted the manuscript.

Acknowledgements
Thanks are specially due to N.Behrnd of Idorsia Pharmaceuticals Ltd. at Allschwil (Switzerland) for help to develop DW macros and 2D conformer conservation issues. This work is dedicated to the memory of Dr.Michel Bremont (INRA, Paris, France) and Dra.Amparo Estepa (UMH, Elche, Spain).

References

[1]Skall, H.F., *et al.* Viral haemorrhagic septicaemia virus in marine fish and its implications for fish farming--a review.*J Fish Dis.* 2005, 28: 509-29 http://dx.doi.org/10.1111/j.1365-2761.2005.00654.x.

[2]Brudeseth, B.E. and Evensen, O. Occurrence of viral haemorrhagic septicaemia virus (VHSV) in wild marine fish species in the coastal regions of Norway.*Dis Aquat Organ.* 2002, 52: 21-8 http://dx.doi.org/10.3354/dao052021.

[3]Schutze, H., *et al.* Complete genomic sequence of viral hemorrhagic septicemia virus, a fish rhabdovirus.*Virus Genes.* 1999, 19: 59-65 http://dx.doi.org/10.1023/a:1008140707132.

[4]Hill, B.J. Physico-chemical and serological characterization of five rhabdoviruses infecting fish.*J Gen Virol.* 1975, 27: 369-78 http://dx.doi.org/10.1099/0022-1317-27-3-369.

[5]Lorenzen, N. and LaPatra, S.E. Immunity to rhabdoviruses in rainbow trout: the antibody response.*Fish & Shellfish Immunology.* 1999, 9: 345-360 http://dx.doi.org/10.1006/fsim.1999.0194.

[6]Salonius, K., *et al.* The road to licensure of a DNA vaccine.*Current Opinion in Investigational Drugs.* 2007, 8: 635-641

[7]Walker, P.J. and Kongsuwan, K. Deduced structural model for animal rhabdovirus glycoproteins.*J Gen Virol.* 1999, 80 (Pt 5): 1211-1220 http://dx.doi.org/10.1099/0022-1317-80-5-1211.

[8]Ahne, W., *et al.* Spring viremia of carp (SVC).*Dis Aquat Organ.* 2002, 52: 261-72 http://dx.doi.org/10.3354/dao052261.

[9]Roche, S., *et al.* Crystal structure of the low-pH form of the vesicular stomatitis virus glycoprotein G.*Science.* 2006, 313: 187-191 http://dx.doi.org/10.1126/science.1127683.

[10]Roche, S., *et al.* Structure of the prefusion form of the vesicular stomatitis virus glycoprotein G.*Science.* 2007, 315: 843-848 http://dx.doi.org/10.1126/science.1135710.

[11]Baquero, E., *et al.* Structure of the low pH conformation of Chandipura virus G reveals important features in the evolution of the vesiculovirus glycoprotein.*PLoS Pathog.* 2015, 11: e1004756 http://dx.doi.org/10.1371/journal.ppat.1004756.

[12]Baquero, E., *et al.* Structural intermediates in the fusion-associated transition of vesiculovirus glycoprotein.*EMBO J.* 2017, 36: 679-692 http://dx.doi.org/10.15252/embj.201694565.

[13]Yang, F., *et al.* Structural Analysis of Rabies Virus Glycoprotein Reveals pH-Dependent Conformational Changes and Interactions with a Neutralizing Antibody.*Cell Host Microbe.* 2020, 27: 441-453 e7 http://dx.doi.org/10.1016/j.chom.2019.12.012.

[14]Carneiro, F.A., *et al.* Membrane fusion induced by vesicular stomatitis virus depends on histidine protonation.*J Biol Chem.* 2003, 278: 13789-94 http://dx.doi.org/10.1074/jbc.M210615200.

[15]Ferlin, A., *et al.* Characterization of pH-sensitive molecular switches that trigger the structural transition of vesicular stomatitis virus glycoprotein from the postfusion state toward the prefusion state.*J Virol.* 2014, 88: 13396-409 http://dx.doi.org/10.1128/JVI.01962-14.

[16]Bearzotti, M., *et al.* The glycoprotein of viral hemorrhagic septicemia virus (VHSV): antigenicity and role in virulence.*Vet Res.* 1995, 26: 413-22

[17]Mourton, C., *et al.* Antigen-capture ELISA for viral haemorrhagic septicaemia virus serotype I.*J Virol Methods.* 1990, 29: 325-33 http://dx.doi.org/10.1016/0166-0934(90)90059-o.

[18]Rocha, A., *et al.* Conformation- and fusion-defective mutations in the hypothetical phospholipid-binding and fusion peptides of viral hemorrhagic septicemia salmonid rhabdovirus protein G.*J Virol.* 2004, 78: 9115-22 http://dx.doi.org/10.1128/JVI.78.17.9115-9122.2004.

[19]Estepa, A. and Coll, J.M. Pepscan mapping and fusion-related properties of the major phosphatidylserine-binding domain of the glycoprotein of viral hemorrhagic septicemia virus, a salmonid rhabdovirus.*Virology.* 1996, 216: 60-70 http://dx.doi.org/10.1006/viro.1996.0034.

[20]Chico, V., *et al.* Pepscan mapping of viral hemorrhagic septicemia virus glycoprotein G major lineal determinants implicated in triggering host cell antiviral responses mediated by type I interferon.*J Virol.* 2010, 84: 7140-50 http://dx.doi.org/10.1128/JVI.00023-10.

[21]Garcia-Valtanen, P., *et al.* Autophagy-inducing peptides from mammalian VSV and fish VHSV rhabdoviral G glycoproteins (G) as models for the development of new therapeutic molecules.*Autophagy.* 2014, 10: 1666-80 http://dx.doi.org/10.4161/auto.29557.

[22]Battles, M.B., *et al.* Molecular mechanism of respiratory syncytial virus fusion inhibitors.*Nat Chem Biol.* 2016, 12: 87-93 http://dx.doi.org/10.1038/nchembio.1982.

[23]Balmer, B.F., *et al.* Inhibition of an Aquatic Rhabdovirus Demonstrates Promise of a Broad-Spectrum Antiviral for Use in Aquaculture.*J Virol.* 2017, 91: http://dx.doi.org/10.1128/JVI.02181-16.

[24]Qin, J.C., *et al.* In vitro and in vivo inhibition of a novel arctigenin derivative on aquatic rhabdovirus.*Virus Res.* 2022, 316: 198798 http://dx.doi.org/10.1016/j.virusres.2022.198798.

[25]Liu, L., *et al.* Inhibition of a novel coumarin on an aquatic rhabdovirus by targeting the early stage of viral infection demonstrates potential application in aquaculture.*Antiviral Res.* 2020, 174: 104672 http://dx.doi.org/10.1016/j.antiviral.2019.104672.

[26]Li, B.Y., *et al.* Quinoline, with the active site of 8-hydroxyl, efficiently inhibits Micropterus salmoides rhabdovirus (MSRV) infection in vitro and in vivo.*J Fish Dis.* 2022, 45: 895-905 http://dx.doi.org/10.1111/jfd.13615.

[27]Bryant, P., *et al.* Structure prediction of protein-ligand complexes from seqeunce information with Umol.*bioRxiv.* 2023: http://dx.doi.org/10.1101/2023.11.03.565471.

[28]Tang, S., *et al.* Accelerating AutoDock Vina with GPUs.*Molecules.* 2022, 27: http://dx.doi.org/10.3390/molecules27093041.

[29]Belot, L., *et al.* Structural and cellular biology of rhabdovirus entry.*Adv Virus Res.* 2019, 104: 147-183 http://dx.doi.org/10.1016/bs.aivir.2019.05.003.

[30]Chen, W.C., *et al.* 4'-(8-(4-Methylimidazole)-octyloxy)-arctigenin: The first inhibitor of fish rhabdovirus glycoprotein.*Fish Shellfish Immunol.* 2023, 139: 108920 http://dx.doi.org/10.1016/j.fsi.2023.108920.

[31]Wahl, J., *et al.* Accuracy evaluation and addition of improved dihedral parameters for the MMFF94s.*J Cheminform.* 2019, 11: 53 http://dx.doi.org/10.1186/s13321-019-0371-6.

[32]Coll, J.M. Evolutionary-docking targeting bacterial FtsZ.*ChemRxiv.* 2023, https://chemrxiv.org/engage/chemrxiv/article-details/6405c36fcc600523a3bcb679: http://dx.doi.org/10.26434/chemrxiv-2023-ld9d3

[33]Coll, J. Star-shaped Triazine-derivatives: would they crossbind SARS-CoV-2 spike helices?*ChemRxiv.* 2021, https://chemrxiv.org/engage/chemrxiv/article-details/6133c1096563696d9d222bbd: http://dx.doi.org/10.33774/chemrxiv-2021-xb6sx-v2.

[34]Lorenzo, M.M., *et al.* Would it be possible to stabilize prefusion SARS-COV-2 spikes with ligands?*ChemRxiv.* 2021: http://dx.doi.org/10.26434/chemrxiv.13453919.v2.

[35]Bermejo-Nogales, A., *et al.* Computational ligands to VKORC1s and CYPs. Could they predict new anticoagulant rodenticides?*BioRxiv.* 2021: http://dx.doi.org/10.1101/2021.01.22.426921.

[36]Che, X., *et al.* An accurate and universal protein-small molecule batch docking solution using Autodock Vina.*Results in enginneering.* 2023, 19: 101335 http://dx.doi.org/10.1016/j.rineng.2023.101335.

[37]Mock, M., *et al.* AI can help to speed up drug discovery - but only if we give it the right data.*Nature.* 2023, 621: 467-470 http://dx.doi.org/10.1038/d41586-023-02896-9.

[38]Coll, J.M. Exploring non-toxic co-evolutionary docking.*ChemRxiv.* 2023, https://chemrxiv.org/engage/chemrxiv/article-details/6512b162ade1178b2424c325: http://dx.doi.org/10.26434/chemrxiv-2023-rr5b0.

[39]Bello-Perez, M., *et al.* SARS-CoV-2 ORF8 accessory protein is a virulence factor.*mBio.* 2023, 14: e0045123 http://dx.doi.org/10.1128/mbio.00451-23.

[40]Dallakyan, S. and Olson, A.J. Small-molecule library screening by docking with PyRx.*Methods Mol Biol.* 2015, 1263: 243-50 http://dx.doi.org/10.1007/978-1-4939-2269-7_19.

[41]Morris, G.M., *et al.* AutoDock4 and AutoDockTools4: Automated docking with selective receptor flexibility.*J Comput Chem.* 2009, 30: 2785-91 http://dx.doi.org/10.1002/jcc.21256.

[42]Huey, R., *et al.* A semiempirical free energy force field with charge-based desolvation.*J Comput Chem.* 2007, 28: 1145-52 http://dx.doi.org/10.1002/jcc.20634.

[43]Trott, O. and Olson, A.J. AutoDock Vina: improving the speed and accuracy of docking with a new scoring function, efficient optimization, and multithreading.*J Comput Chem.* 2010, 31: 455-61 http://dx.doi.org/10.1002/jcc.21334.

[44]Coll, J.M. New star-shaped ligands generated by evolutionary fitting the Omicron spike inner-cavity.*ChemRxiv.* 2023, https://chemrxiv.org/engage/chemrxiv/article-details/6479b8cfbe16ad5c57577cce: http://dx.doi.org/10.26434/chemrxiv-2023-v8qqj

[45]Coll, J.M. Anticoagulant rodenticide novel candidates predicted by evolutionary docking.*ChemRxiv.* 2023, https://chemrxiv.org/engage/chemrxiv/article-details/6479b8cfbe16ad5c57577cce: http://dx.doi.org/10.26434/chemrxiv-2023-gh4xl-v2.

[46]Coll, J. Could Acinetobacter baumannii Lol-abaucin docking be improved?*ChemRxiv.* 2023, https://chemrxiv.org/engage/chemrxiv/article-details/649aa71aba3e99daef1d1756: http://dx.doi.org/10.26434/chemrxiv-2023-962ht.

[47]J.M., C. Generation of ligands to F13L mutations isolated in MonkeyPoxVirus-infected patients resistant to Tecovirimat-treatment.*ChemRxiv.* 2024, http://dx.doi.org/10.26434/chemrxiv-2024-bc9cx:

[48]Bello-Perez, M. and Coll, J.M. Ligands docking to ORF8 by co-evolution. Could they reduce the inflammation levels induced by SARS-COV-2 infections?*ChemRxiv.* 2023, https://chemrxiv.org/engage/chemrxiv/article-details/655f2f3629a13c4d47ced2aa: http://dx.doi.org/10.26434/chemrxiv-2023-6r8s7.

[49]Estepa, A.M., *et al.* A protein G fragment from the salmonid viral hemorrhagic septicemia rhabdovirus induces cell-to-cell fusion and membrane phosphatidylserine translocation at low pH.*J Biol Chem.* 2001, 276: 46268-75 http://dx.doi.org/10.1074/jbc.M108682200.